Assessment of RC walls with cut-out openings strengthened by FRP composites using a rigid-plastic approach

Abstract

Building refurbishment works frequently require the cutting of new openings in concrete walls. Cutting new openings weakens the overall response of such elements, so they usually require strengthening. However, current design codes offer little guidance on strengthening walls with openings, and less still on the use of non-metallic reinforcements such as FRP (Fibre Reinforced Polymers) to ensure sufficient load bearing capacity. This paper proposes a new procedure based on limit analysis theory for evaluating the ultimate load of walls with cut-out openings that have been strengthened with carbon-FRP (CFRP). First, the approach is verified against transverse (out-of-plane) and axial (in-plane) loading for unstrengthened specimens. These loading types result in different failure mechanisms: transverse loading leads to failure due to yielding/rupture of the steel reinforcement while axial loading leads to failure by concrete crushing. Second, the proposed method is further developed for CFRP-strengthened specimens under axial loading. It accounts for the contribution of CFRP indirectly, by updating the concrete model with an enhanced compressive strength as a result of confining the piers. Predictions made using the new method agree closely with experimental results.

Author keywords: Walls with openings, Eccentric axial loading, Transverse loading, Concrete plasticity, Effectiveness factor, Strengthening, Fibre-reinforced polymers

Assessment of RC walls with cut-out openings strengthened by FRP composites using a rigid-plastic approach

Cosmin Popescu[a,*]; **Jacob W. Schmidt**[b]; **Per Goltermann**[b]; and **Gabriel Sas**[c]

[a] Northern Research Institute – NORUT, Rombaksveien E6-47, N-8517 Narvik, Norway
[b] Technical Univ. of Denmark, Dept. of Civil Engineering, Building 118, DK-2800 Kgs. Lyngby, Denmark
[c] Luleå Univ. of Technology, Dept. of Civil, Environmental and Natural Resources Engineering, SE-97187, Luleå, Sweden

* Corresponding author. Tel.: +46 702375433.
E-mail addresses: cosmin.popescu@norut.no (C. Popescu), jws@byg.dtu.dk (J.W. Schmidt), pg@byg.dtu.dk (P. Goltermann), gabriel.sas@ltu.se (G. Sas)
(G. Sas).

Abstract

Building refurbishment works frequently require the cutting of new openings in concrete walls. Cutting new openings weakens the overall response of such elements, so they usually require strengthening. However, current design codes offer little guidance on strengthening walls with openings, and less still on the use of non-metallic reinforcements such as FRP (Fibre Reinforced Polymers) to ensure sufficient load bearing capacity. This paper proposes a new procedure based on limit analysis theory for evaluating the ultimate load of walls with cut-out openings that have been strengthened with carbon-FRP (CFRP). First, the approach is verified against transverse (out-of-plane) and axial (in-plane) loading for unstrengthened specimens. These loading types result in different failure mechanisms: transverse loading leads to failure due to yielding/rupture of the steel reinforcement while axial loading leads to failure by concrete crushing. Second, the proposed method is further developed for CFRP-strengthened specimens under axial loading. It accounts for the contribution of CFRP indirectly, by updating the concrete model with an enhanced compressive strength as a result of confining the piers. Predictions made using the new method agree closely with experimental results.

Author keywords: Walls with openings, Eccentric axial loading, Transverse loading, Concrete plasticity, Effectiveness factor, Strengthening, Fibre-reinforced polymers

1. Introduction

Precast concrete walls are commonly used as load-bearing elements for low- to mid-rise structures. The popularity of such elements is due to their efficient construction and design flexibility. Openings for doors and/or windows can be readily accommodated by carefully considering the effects of their presence during the design stage and addressing any weaknesses they may introduce by specifying appropriate reinforcement detailing around their edges. However, problems frequently arise when such structures are refurbished and new openings (i.e. cut-out openings) are introduced to facilitate changes in role, for example when apartment buildings are converted into office spaces. These openings introduce weaknesses that can reduce the wall's overall performance in terms of flexural and/or axial strength, stiffness, and energy dissipation. Consequently, repairs (defined here as actions that fully or partially restore the structure's load-carrying capacity) using fibre-reinforced polymers (FRP) are often required. However, before a repair method can be used with confidence, it is necessary to have reliable information on the degree to which the un-strengthened wall has been weakened.

Although there have been many experimental studies on the behaviour of reinforced concrete (RC) walls, the performance of RC walls with openings has not been investigated in the same depth. The few studies that have been published in this area [1-6] have focused on structural walls subjected to seismic forces (constant axial load + lateral loading to failure). Walls designed for non-seismic applications, which must primarily withstand axial compression loads (i.e. axial loading to failure with no transverse loads between supports or lateral in-plane forces) are equally important but have received much less research attention. The literature on the behaviour of axially loaded walls was recently reviewed by Popescu et al. [7]. It was concluded that most reported tests have focused on the behaviour of one-way walls [8-13], i.e. walls that are restrained along the top and bottom edges and thus develop a uniaxial curvature. Fewer tests have been conducted on walls under two-way action [11, 14-16], i.e. walls that are restrained along all edges and thus developing a biaxial curvature, and walls with openings [17-20].

Efforts have also been made to develop design models capable of predicting the axial capacity of such elements. Most such models are empirical and calibrated using data from limited numbers of one-way and two-way action tests, with loading eccentricities of up to one sixth of the wall's thickness. These design models account for the contribution of the reinforcement [9, 12, 16], high-strength concrete and increasing slenderness [21], material nonlinearities [13, 22, 23], and the presence of the opening [17, 18, 24]. Numerical models have been proposed in different studies, [24-26], in an attempt to investigate through parametric studies, the influence of slenderness and aspect ratios, concrete strength, eccentricities, reinforcement ratios, as well as various boundary conditions.

Major design codes such as EN1992-1-1 [27], ACI 318 [28] and AS3600 [29] also offer design models. These models were initially developed for one-way walls but restraining factors were subsequently introduced into the European [27] and Australian [29] design codes on the basis of German work [30]. These restraining factors account for the effects of restraining the lateral edges (i.e. two-way action) by reducing the wall's effective height based on the boundary conditions.

A review that evaluated existing design methods using a database covering 253 tests on one- and two-way walls under axial loading (with and without openings) [7] found that "design models established in design codes provide the most conservative results, while those proposed in other studies [13, 16, 17, 31] showed a certain level of non-conservatism". Moreover, the authors were only able to identify a single published study on the use of carbon-FRP (CFRP) to strengthen axially loaded concrete walls with cut-out openings [20]. Unfortunately, this study only considered one-way walls, so the associated design model is only valid for such walls.

Because empirical models have certain shortcomings (for example, they rely on coefficients obtained by curve-fitting using data from a specific experimental setup), their application in practical contexts is likely to give rise to considerable scatter on both the safe and unsafe sides. Therefore, there is a clear need for a theory-based method that can describe biaxial effects on panels restrained on all sides and also account for the effects of openings and the contributions of FRP strengthening materials. This manuscript describes the development of such a general analytical method based on limit analysis and concrete plasticity. Experiments conducted by the authors at Luleå University of Technology and the Technical University of Denmark provided the model's foundations, and the results of these studies are briefly summarized here.

2. Overview of the experimental tests

During service, RC walls must withstand various kinds of loads, including (1) gravitational loads parallel to the mid-surface at a given eccentricity due to construction errors; (2) horizontal out-of-plane forces due to wind loads; (3) handling, transportation and erection loads, and potentially (4) accidental loads such as seismic or blast loads. Loads of the first two classes are usually the governing load cases for structures erected in non-seismic regions and are therefore the focus of this study (Figure 1). The results of experiments on two-way walls under lateral (out-of-plane) bending [32] and under eccentric uniaxial compression [33, 34] will be briefly summarized in this section. Both experimental programmes include walls with symmetric openings that replicate solid walls with sawn cut-outs, i.e. no additional reinforcement was placed around the edges or corners of the openings. An overview of the main properties of the tested walls is given in Table 1.

2.1. Transversally loaded walls

An experimental program was conducted in which six full-scale lightly-reinforced concrete walls (4 m × 2.6 m × 0.1 m) were subjected to uniform transverse loading. The applied force was fully distributed on the wall surface using airbags that react against a backing steel frame (Figure 2). The walls' vertical and horizontal edges were simply supported, i.e. restrained against translation while allowing rotation. No vertical pre-compression other than their own weight was applied to the tested specimens. Parameters varied across the tested specimens include the reinforcement ratio and the presence of a window opening. The reinforcement consisted of a single wire mesh of deformed bars with 150 mm spacing in both orthogonal directions (ϕ6/150 for specimens A, B, C and D, or ϕ5/150 for specimens E and F); the vertical and horizontal steel reinforcement ratios resulting from this configuration are given in Table 1. The wire mesh was offset from the mid-surface towards the tension side of the wall to achieve a concrete cover of about 30 mm.

2.2. Axially loaded walls

Half-scale walls designed to represent typical wall panels in residential buildings, with and without cut-out openings (1.8 m × 1.35 m × 0.06 m), were constructed for testing to failure. The walls were tested in two-way action and subjected to axial loading (with no transverse loads between supports or lateral in-plane forces) with low eccentricity along the weak axis (1/6th of the wall's thickness) to represent imperfections due to thickness variation and misalignment of the panels during the construction process. The two-way action refers to the specimens' boundary conditions, and was imposed using a steel test rig (Figure 3). The test rig featured (1) top and bottom restraints to simulate a hinge connection that allowed full free rotation and to apply eccentric loading through a steel rod welded to each loading beam (Figure 4); and (2) lateral restraints to simulate the effect of transverse walls that permit rotation but prevent translation (Figure 4).

The test matrix can be divided into three stages, designated I-III. Three specimens were loaded to failure in stage I: a solid wall (I-C), a wall with a “small” symmetric single door opening (I-S), and a panel with a “large” symmetric double door opening (I-L). In stage II, two specimens [one with a small opening (II-S) and one with a large opening (II-L)] were first precracked and then strengthened with CFRP before being tested to failure. The precracking level was determined by loading the specimens to the point required to create a significant crack. The significance of a crack depends on many factors, including the building’s function and environmental exposure class. However, ACI 224R-01 [35] states that a crack wider than 0.15 mm may require repair, so this value was used to define cracking loads. To create cracks of this width, the specimens were loaded at up to 75% of their unstrengthened axial capacity. In stage III, duplicate specimens with openings of each size were strengthened with the CFRP system in an uncracked state and then loaded to failure. It should be noted that “small” and “large” are used here as convenient designations rather than clearly delimited terms with specific thresholds and implications.

All specimens were reinforced with welded wire fabric (ϕ5/100 in both orthogonal directions) placed centrally in a single layer. The dimensions of the reinforcement mesh were measured from edge to edge of the concrete wall (i.e. bars were cut off with no additional anchorage provided at the specimen’s edges such as bends or hooks). The specimens’ dimensions and details of their reinforcement are presented in Figure 5.

Uniaxial U-shaped CFRP laminates covering the wall’s entire surface and fixed in place with mechanical anchorages were used for strength enhancement. Before applying the CFRP strengthening, 8 mm holes were drilled through the wall at positions marked on the concrete surface to facilitate the installation of the mechanical anchorages. The concrete surfaces were then prepared by grinding to remove irregularities and the cement paste layer, exposing the aggregates, and then by cleaning with compressed air. The CFRP fabrics were applied using the wet lay-up procedure. First, a two-component epoxy primer was applied to the specimens, followed by the application of the impregnated fibres to the concrete surface after approximately 6 hours. The fibres were wrapped around the piers in a U-shape; full wrapping was not possible due to the boundary conditions (see Figure 3). The CFRP laminates were placed along both lateral faces from one edge of the wall to the other, and bent under the bottom part of the beam. High-strength CFRP (StoFRP Sheet IMS300 C300) was used as the bonded material, and **was** impregnated using a two-component epoxy resin (StoPox LH). A week later, when the epoxy had cured, the anchorage bolts were inserted into predrilled holes and prestressed with a torque equal to 75% of the proof load (the estimate was based on the clamp load of 8.7 kN), as specified in SS-EN ISO 898-1 [36]. The material properties of the CFRP system are specified in Table 2.

The strengthening system was designed in accordance with the FRP-confinement design model proposed by Lam and Teng [37]. An estimate of the required thickness of the CFRP jacket was obtained by arranging the mechanical anchorages in a configuration that created vertical strips with a cross-sectional aspect ratio that was limited to 2:1 (60 x 120 mm2, as shown in Figure 6). The addition of the CFRP laminates should increase the concrete's compressive strength to the value (f_{cc}) required to ensure that the strengthened walls' load bearing capacity matches that of the original solid wall. Two and three CFRP plies were used to strengthen the specimens with small and large openings, respectively. The fabric architecture and the lamination schedule are illustrated in Figure 6. The results obtained from the empirical model [37] – developed for pure axial loads – may deviate from real values in cases where eccentricities exist. The authors are aware that the eccentric loading applied to the tested specimens may reduce the effectiveness of the confinement, but the lack of better models prevented the incorporation of appropriate parameters to simulate its effects. The discussion in this section focuses on the pre-test design procedure (including its limitations); the development of a new model and post-test predictions are presented in Section 3.

3. Design for ultimate strength and comparison with tests

3.1. Failure mechanism

The failure mechanism of unstrengthened walls under transverse loads is virtually identical to that of a slab unless the contribution of vertical loads is very important. Bailey and Toh [38] showed that two distinct failure modes can occur for transversally loaded slabs depending on the reinforcement ratio. This parameter is defined by the ultimate tensile force of the reinforcement relative to the compressive force of the concrete across the thickness of the slab [38], and is computed using the following expression:

$$\rho = \frac{1}{2}\left[\left(\frac{f_{u,x}A_{s,x}}{0.8 f_c d_x}\right)+\left(\frac{f_{u,y}A_{s,y}}{0.8 f_c d_y}\right)\right] \quad (1)$$

Bailey's experimental observations yielded a threshold value for the parameter ρ, which delineates the transition point from failure due to reinforcement fracture ($\rho < 0.08$) to failure due to concrete crushing ($\rho > 0.08$). However, this threshold is only valid for square plates; further tests are required to define a suitable threshold value for rectangular plates. For the specimens tested in this work, the reinforcement ratio calculated according to Eq. (1) for transversally loaded walls is 0.05. In the case of solid walls, the failure mechanism involved the formation of cracks extending from approximately the centre of the wall towards the corners at an angle of approximately 45° to the floor; in walls with openings, failure occurred via the formation of diagonal cracks extending from the corners of the opening to the closest corner of the wall as shown in Figure 7a. The experimental results indicated that the reinforcement fractured along the yield lines, confirming Bailey's conclusions. The failure mechanism is ductile, and the associated displacements are large (see Table 1).

Crack propagation is significantly influenced by the dominant load (transverse vs. axial loading), but the crack pattern at the ultimate load was independent of the loading strategy, as illustrated in Figure 7b. The failure process for walls under eccentric axial loads started from the corners of the wall – the concrete initially cracked on the tension side of the wall, with subsequent concrete crushing on the compression side along the major cracks. The failure mechanism (which is due to the second order effect) is brittle, and the associated displacements are relatively small (see Table 1). Double curvature in both the horizontal and vertical directions of the walls was observed in the experiments. This indicates that, in contrast to the typical assumptions of design codes, the lateral restraints make the problem bi-dimensional rather than one-dimensional. The addition of CFRP (for strengthened walls) did not appear to change the position of the yield lines prior to failure. After that point, as seen in Figure 8 the failure became localized along the bottom of the piers due to crushing of the concrete, which caused the covering CFRP mesh to be torn away from the wall. The CFRP strengthening increased the axial capacity of walls with small and large openings by 34 – 50% and 13 – 27%, to 85 – 95% and 57 – 63% of their pre-cutting capacity (i.e. solid wall), respectively.

The major cracks shown in Figure 7 define the geometrical models (yield lines) related to the corresponding failure mechanisms. Figure 9a shows the yield lines observed for walls under transverse loading; those for walls under axial loading are illustrated in Figure 9b.

3.2. Yield conditions

This section describes the yield conditions for all of the constituent materials included in the analysis, i.e. concrete, steel reinforcement and FRP. Qualitative depictions of the real and idealized stress-strain laws for each material are presented in Figure 6. However, the use of limit analysis requires the implicit assumption that materials exhibit perfect plasticity with idealized failure criteria, as shown in Figure 6. Elastic displacements are neglected, which implies rigid behaviour until the plastic plateau is reached.

3.2.1. Concrete

The concrete is assumed to behave according to the modified Coulomb criterion with tensile strength accounted for using a zero tensile cut-off but otherwise neglected (see Figure 6a). The ultimate strength of concrete under uniaxial stress state must be reduced to an equivalent plastic compressive strength (Level I in Figure 10a) using an effectiveness factor $\nu < 1$ because of the material's brittleness and the influence of transverse strains on the concrete's strength [39]. According to the fib Model Code 2010 [39], the effectiveness factor can be expressed as the product of η_{fc} and η_{ε} – strength reduction factors reflecting the brittleness of concrete and the influence of transverse cracking, respectively. The equivalent plastic compressive strength for unconfined concrete is the product of f_c and ν:

$$\nu = \eta_{fc} \cdot \eta_{\varepsilon} \qquad (2)$$

where η_{fc} is defined as:

$$\eta_{fc} = \left(\frac{f_{c0}}{f_c} \right)^{1/3} \leq 1.0 \qquad (3)$$

with f_{c0}=30 MPa, and η_{ε}=0.55 for compression bands with reinforcement running obliquely to the direction of compression.

3.2.2. Steel reinforcement

The steel reinforcement was also assumed to behave in a rigid-plastic manner in both tension and compression, as shown in Figure 10b. Two values for the plastic plateau were selected, representing two different cases. In the first case, the plateau corresponds to the yielding point reached in uniaxial tensile tests on reinforcement coupons (see Table 1). In the second case, the plastic plateau is defined as the tensile strength reached in uniaxial tensile tests on reinforcement coupons (see Table 1). The reason for using the tensile strength as the plastic plateau rather than the yield strength of the material will be discussed later.

3.2.3. Fibre-reinforced polymers

The real behaviour of the non-metallic reinforcement, i.e. CFRP, is linear elastic, with no plasticity or softening branch (Figure 10c). Consequently, the assumption of rigid-plastic behaviour becomes questionable. In an attempt to account for the contribution of CFRP in strengthened slabs with openings, Floruţ et al. [40] used the strength corresponding to the debonding strain as observed in experimental tests. An alternative procedure proposed in this paper is to update the concrete model using an enhanced confined compressive strength (f_{cc}) due to FRP confinement. The procedure is based on the following expressions, as discussed previously [37]:

$$f_{cc} = \left(1 + k_1 k_{s1} \frac{f_l}{f_c}\right) f_c \tag{4}$$

where k_1=3.3 is the confinement effectiveness coefficient, k_{s1} is a parameter used to account for the effect of the non-uniformity of confinement according to Eq. (5), and f_l is the confining pressure defined by Eq. (6).

$$k_{s1} = \left(\frac{b}{t}\right)^2 \frac{A_e}{A_c} \tag{5}$$

$$f_l = \frac{2 f_{frp} n_{plies} t_{frp}}{\sqrt{b^2 + h^2}} \tag{6}$$

and,

$$\frac{A_e}{A_c} = \frac{1 - \left[\left(b/h\right)(h-2R)^2 + (h/b)(b-2R)^2\right]/3A_g - \rho_{sc}}{1 - \rho_{sc}} \tag{7}$$

where b and h are width and height of the cross-section, respectively, A_e is the effective confinement area, A_c is the total area of the cross-section, R is the corner radius, ρ_{sc} is the cross-sectional area proportion of longitudinal steel, and A_g is the gross area of the column section with rounded corners.

The model discussed above is valid only for pure axial loads, but the specimens in this work were loaded with small eccentricities to simulate the effects of the imperfections that occur in normal construction practices. Therefore, the effectiveness factor should incorporate an additional parameter to account for eccentricity and slenderness effects. The impact of these effects is demonstrated by the difference between the strain readings obtained on the tension (e.g. F1-T) and compression (e.g. F1-C) sides of the specimens, as shown in Figure 11. To illustrate this point, ultimate strain readings are presented for specimens II-S (Figure 11a) and II-L (Figure 11b).

The transformation factor from non-uniform confinement to uniform confinement was calculated as the ratio of the average and maximum strain at each measurement point according to Eq. (8):

$$\eta_{\varepsilon,frp} = \frac{\varepsilon_{avg}}{\varepsilon_{u,frp-max}} \leq 1.0 \tag{8}$$

where,

$$\varepsilon_{avg} = \frac{\varepsilon_{u,frp-max} + \varepsilon_{u,frp-min}}{2} \tag{9}$$

It should be noted that these values are locally measured strains that may be affected by stress concentrations or by being offset from the maximum values of the strain path. Therefore, the transformation factor due to eccentricity was averaged over points F1-F4 for all specimens tested, yielding values of approximately 0.75 and 0.55 for walls with small and large openings, respectively. A new expression for the equivalent plastic compressive strength that incorporates the new strength reduction factor ($\eta_{\varepsilon,frp}$) was then defined: Eq. (10).

$$\text{Level II} \rightarrow \eta_{fc} \cdot \eta_{\varepsilon} \cdot \left(f_c + \eta_{\varepsilon,frp} \cdot \Delta f \right) \tag{10}$$

Here, Δf is the difference in compressive strength between unconfined and CFRP-confined concrete.

Unlike $\eta_{\varepsilon,frp}$, the other two strength reduction terms in Eq. (10) are calculated in the same way as for un-strengthened walls. The difference is that the compressive strength is replaced with the confined compressive strength in Eq. (3) and the effect of transverse strain is conservatively treated as being unchanged. However, the addition of extra reinforcement (i.e. CFRP) means that transverse strains are unlikely to produce the same internal damage in concrete. It would therefore be useful to further calibrate the model in future studies.

3.3. Limit analysis approach

The limit analysis theory for slabs (i.e. the yield line method) has been extensively investigated in recent decades. However, there are only a few published examples of its use to predict the ultimate capacity of plain or lightly-reinforced elements with limited ductility. Such elements are typically strengthened with a single layer of reinforcing material, which is used to control cracks formed due to creep, shrinkage and erection/transportation loads. Because of their limited plasticity, the applicability of the limit analysis approach could potentially be questioned. However, it may be relevant in cases where the walls are predominantly subject to out-of-plane bending. The method was first described by Ingerslev [41] and further developed by Johansen [42]. The analysis is performed by means of "virtual work" or using the "equilibrium method". In this paper the virtual work method is used, in which a possible plastic collapse mechanism occurs along predefined yield lines as shown schematically in Figure 9. Usually, multiple collapse mechanisms are tested and the yield line solution is defined as the solution with the lowest load at failure (in assessments) or the highest moments (during design processes). The process in this work was simplified by considering only the collapse mechanism observed in the tests, which involves the formation of wide cracks (fracture lines) as shown in Figure 7. These fracture lines indicate the positions of the positive yield lines that divide the plates into rigid disks and thereby dissipate energy. The method assumes that the work dissipated along the yield lines (i.e. the internal work) is equal to the work done by the applied loads (i.e. the external work). This assumption yields a work equation of the following form:

$$\sum\left(\iint S_u \delta dxdy\right)_{\text{each region}} = \sum\left(\int m_b \theta ds\right)_{\text{each yield line}} \qquad (11)$$

where the integrals on the left- and right-hand sides represent the external and internal work, respectively, with S_u denoting the uniformly distributed load per unit area, δ the virtual displacement, m_b the bending moment, and θ the rotation of the region about its axis of rotation. Equation (11) represents the classical solution valid for plates loaded perpendicular to the elements' mid-plane. In walls where vertical forces will affect the external work and the corresponding strength components, the out-of-plane loads may be accompanied by in-plane loads. A diagram used to develop a work equation applicable to such situations is presented in Figure 12.

The work equation now becomes:

$$\sum\left(\iint S_u \delta dxdy\right)_{\text{each region}} - \int\left(n_{ux,uy} \delta dx, y\right)_{\text{each boundary}} = \sum\left(\int m_b \theta ds\right)_{\text{each yield line}} \qquad (12)$$

where n_{ux} and n_{uy} are the uniform in-plane compressive forces per unit length applied in the x- (horizontal) and y- (vertical) directions, respectively. To compare the predicted loads to the available experimental data, these compressive forces are applied eccentric to the mid-plane of the wall along its weak axis while forces acting in the x-direction are assumed to be nonexistent. Depending on their magnitude, these compressive forces can either increase the wall's capacity or govern its ultimate failure. Two cases were therefore investigated: (1) $n_{uy} << S_u$, corresponding to dominant transverse loads, and (2) $n_{uy} >> S_u$, corresponding to dominant in-plane vertical loads.

3.4. Case I: Dominant transverse loads

Practical examples of transverse loadings include wind loads, blasts, snow avalanches, and lateral earth pressure. Such loadings are typically unlikely to occur; where they do occur frequently in mid-rise concrete structures (as may be the case for, e.g., wind loads), they are unlikely to become dominant. In addition to the uniformly distributed loads acting perpendicularly to the wall mid-plane, the walls may be subjected to other loads such as gravitational loads. These are expected to increase the walls' ultimate capacity due to the favourable contribution of non-negligible and constant gravitational loads. However, in cases where the axial load derives solely from the self-weight, the additional contribution tends to be small. Previous investigations on masonry walls [43] found that self-weight accounted for less than 10% of the ultimate load in simply supported walls, so the self-weight contribution was disregarded when comparing theoretical predictions to experimental data.

The external and internal work can be obtained using Eq. (12) and used to derive a failure load, leading to the following expressions:

- for the solid wall

$$S_u = \frac{2m_b\left(H/L_x + 2L/H\right)}{\left[\left(L/2 - L_x/3\right)\right]H} \tag{13}$$

- for the wall with an opening

$$S_u = \frac{4m_b\left(H_y/L_x + L_x/H_y\right)}{\left(\frac{4}{3}L_xH_y + H_0L_x + L_0H_y + H_0L_0\right)} \tag{14}$$

The unknown term, L_x, defines the theoretical position of the inclined yield lines. For the solid walls, an exact solution was found by differentiating equation (13) over the term L_x, $\partial S_u/\partial L_x=0$, that is,

$$\frac{12m_b\left[4H^2L_x-3HL+4L\left(L_x\right)^2\right]}{\left(L_x\right)^2\left(-2L_x+3L\right)^2H}=0 \tag{15}$$

which leads to a quadratic solution for L_x with the following positive root:

$$L_x=\frac{1}{2}\frac{\left(-H+\sqrt{H^2+3L^2}\right)H}{L} \tag{16}$$

Solving Eq. (16) provides the slope of the yield line, which is predicted to intersect with the corners of the wall at 40º; this is consistent with the average angle observed experimentally in the crack patterns at failure. Openings, when present, tend to attract yield lines [44]. Thus, in specimens with openings, the yield lines of a solid wall are interrupted by cracks connecting the corners of the wall to the closest corner of the opening, as shown in Figure 9a.

The reinforcement contributes to the internal work. It is accounted for in the work equation by first considering the equilibrium condition shown in Figure 13 to determine the bending moment m_b.

$$m_bL=\left(m_x\cdot L\sin\alpha\right)\sin\alpha+\left(m_y\cdot L\cos\alpha\right)\cos\alpha \tag{17}$$

$$m_b=m_x\sin^2\alpha+m_y\cos^2\alpha \tag{18}$$

where m_x, m_y are the moment capacities per unit width in the x- and y-directions, respectively, expressed as follows:

$$m_{x,y}=\left(1-\frac{1}{2}\frac{A_{sx,sy}f_y}{sdf_c}\right)\frac{dA_sf_y}{s} \tag{19}$$

where A_{sx}, A_{sy} are the areas of the reinforcement per unit width in the *x*- and *y*-directions, respectively, f_y is the yield strength of the reinforcement, *d* is the effective depth, and *s* is the reinforcement spacing. In the isotropic case (i.e. m_x=m_y), Eq. (18) reduces to m_b=m_x=m_y. For simplicity, the minor differences in the effective depths along the principal directions of the reinforcement are neglected in the following calculations.

The failure capacities predicted by yield line analysis are given in Table 3. These predictions underestimate the capacity in all cases; the average ratio of the theoretically and experimentally determined capacities was 0.85. This may be because the inclusion of lightly reinforced specimens in the tests resulted in some large deflections at failure (see Table 1) with rupture of the steel reinforcement, which limits the applicability of the rigid-plastic approach. The method is most useful when the maximum deflection recorded at failure does not exceed half the wall's thickness, or more precisely, 0.42× the wall's thickness based on the expression of Wang et al. [45] (Eq. 20).

$$w_0 = \sqrt{\frac{0.1 f_y}{E_s} \cdot \frac{3L^2}{8}} \tag{20}$$

Better predictions could be obtained by considering two hidden capacities: (1) strain hardening of the reinforcement, and (2) tensile membrane action (TMA) due to large deflections. While the former only requires updating the yield condition (refer to Figure 10b), i.e. substituting the yield strength with the ultimate strength of the reinforcement, the latter approach would require a more advanced analysis that accounts for the effect of geometric changes. For plates with a central deflection, *w*, greater than w_0, Wang et al. [45] proposed a model that explicitly considers the TMA by including in the equilibrium equation the vertical component that develops in the reinforcement. The use of TMA is usually neglected in common cases on the basis of the lower bound theorem, and is only considered when design is performed against accidental loads, e.g. structures subjected to fire [46]. Consequently, the underprediction of the experimentally measured capacities was addressed by considering the effects of reinforcement strain hardening. Improved predictions taking this factor into account are presented in Table 3.

3.5. Case II: Dominant in-plane vertical loads

In cases where the walls are part of a structure with regular floor plans that carry mainly axial loads, the main contribution to the ultimate capacity comes from the concrete in compression (compressive membrane action - CMA) and the reinforcement. There are few published experimental studies that could shed light on the real contribution of reinforcing materials to the ultimate capacity when applied in a single layer. Moreover, design codes usually neglect the contribution of reinforcement for lightly-reinforced elements where the main purpose of reinforcement is to control cracking due to creep, shrinkage and erection/transportation loads. Given the limited understanding of these issues and the lack of relevant experimental data, the contribution from the reinforcement in such cases was neglected.

Because of the small displacements of the element at failure, a compressive membrane effect develops that depends solely on the concrete's plasticity. This effect can be attributed to the in-plane restraints provided by the vertical edge supports. The membrane moment can be determined by considering a horizontally restrained unreinforced one-way strip that is transversally loaded by two symmetrical line loads as proposed by Nielsen [44]. By considering the maximum deflection exhibited by the experimentally studied walls before undergoing plastic collapse (δ_{peak}) as presented in Table 1, the membrane moment can be expressed as:

$$m_c = \frac{1}{4} f_c \left(t - \delta_{peak}\right)^2 \qquad (21)$$

The derivation of this equation has been presented elsewhere [44] and, for the sake of brevity, will not be reproduced here. The compressive strength of concrete in Eq. (21) is modified by the effectiveness factors calculated according to Eqs. (2) and (10) for unstrengthened walls and walls strengthened with CFRP, respectively. To verify the model against the experimentally tested specimens, the maximum out-of-plane displacements at peak load (δ_{peak}) obtained in the experiments are used in the following calculations. In practice, such parameters are usually difficult to determine accurately without using an iterative process that accounts for material and geometrical nonlinearity as well as the relevant boundary conditions. However, the Australian code [29] provides some practically useful guidance; the theoretical basis of this guidance is outlined elsewhere [11]. The procedure for estimating the deflection at the critical wall section that is described in AS3600 [29], Eq. (22), applies a sinusoidal curvature using deflections obtained from bending-moment theory [47]. These deflections only account for the element's initial stiffness and therefore do not include the nonlinear deflections.

$$\Delta = \frac{\left(H_{eff}\right)^2}{8}\phi_m \tag{22}$$

Here, ϕ_m is a function of the elastic modulus for concrete and the uncracked depth of the cross-section.

$$\phi_m = \frac{\sigma_c / E_c}{x} \tag{23}$$

The elastic modulus of normal strength concrete is assumed to be E_c=1000f_c [11]. Limiting the stress in the concrete (σ_c) to 0.8f_c, and the uncracked depth of the cross-section (x) to t/4 furnishes the following expression for the out-of-plane deflection:

$$\Delta = \frac{\left(H_{eff}\right)^2}{2500t} \tag{24}$$

with $H_{eff}=\beta H$ being the effective height. Values for the effective height factor β are given for the most commonly encountered restraints [29]:

$$\beta = \begin{cases} \dfrac{1}{1+\left(\dfrac{H}{3L}\right)^2} & \text{three sides} \\[2ex] \dfrac{1}{1+\left(\dfrac{H}{L}\right)^2} & \text{four sides with } L \geq H \\[2ex] \dfrac{L}{2H} & \text{four sides with } L < H \end{cases} \tag{25}$$

Equation (24) is valid for unstrengthened specimens, but confining the wall-piers with CFRP laminates will increase the flexural rigidity and thus reduce the deflections. The ratio of the enhanced concrete compressive strength due to confinement relative to the unconfined concrete strength was 1.35 and 1.53 for walls with small and large openings, respectively. By substituting the new values for elastic modulus, Eq. (24) can be rewritten as:

$$\Delta = \begin{cases} \dfrac{\left(H_{eff}\right)^2}{3375t} & \rightarrow \text{CFRP-strengthened wall with small opening} \\[2ex] \dfrac{\left(H_{eff}\right)^2}{3825t} & \rightarrow \text{CFRP-strengthened wall with large opening} \end{cases} \tag{26}$$

As in the case of transversally loaded walls, the work done by the external loads must be balanced by the virtual internal work. As suggested by Nielsen [44], the internal work is determined by replacing the bending moment m_b in the usual yield line solution with the membrane moment m_c. It is difficult to determine exact solutions for the inclined yield lines in such cases; in this work, such solutions were obtained by considering experimental evidence in the first case, and subsequently validated using advanced computational simulations.

Results obtained based on a three-dimensional nonlinear finite element model [48] implemented using ATENA-Science [49] are illustrated in Figure 14. The figure shows the calculated principal plastic strains in concrete on the compression side at failure to support the validity of the plastic mechanism adopted in Figure 9b and the close agreement between predictions based on this mechanism and the experimental observations. No further results based on the computer simulations will be presented in this paper because they have already been described in a separate publication [48]. At ultimate, the magnitude of the principal plastic strains in concrete was capped at a predefined level during post-processing to highlight the possible plastic mechanism. For ease of visualisation, finite elements with strains above this threshold value (50% of the ultimate compressive strain in the concrete, where ε_{cu}=3.2‰) are not displayed. A median line is then drawn through the crushing band, indicating the yield line's inclination. The angles predicted were in close agreement with the experimental observations. The external and internal work for the different kinds of axially loaded walls can be computed using the following expressions:

External work:

$$W_E = \begin{cases} \dfrac{t}{3} n_{uy} L(\theta_1 + \theta_2) & \rightarrow \text{solid wall} \\ \dfrac{t}{3} n_{uy} \dfrac{L - L_0}{2} (\theta_1 + \theta_2) & \rightarrow \text{small opening} \\ \dfrac{t}{3} n_{uy} L_x (\theta_1 + \theta_2) & \rightarrow \text{large opening} \end{cases} \tag{27}$$

Internal work:

$$W_I = \begin{cases} m_c L(\theta_1 + \theta_2) + 2 m_c H \varphi & \rightarrow \text{solid wall} \\ m_c \dfrac{L - L_0}{2} \left(\theta_1 + \theta_2\right) + m_c H \varphi & \rightarrow \text{small opening} \\ m_c L_x \left(\theta_1 + \theta_2\right) + m_c \left(H - H_0 + H_y\right) \varphi & \rightarrow \text{large opening} \end{cases} \tag{28}$$

where for the solid wall $\theta_1 = \theta_2 = 2\delta / H$ and $\varphi = \delta / L_x$; for the wall with small opening $\theta_1 = \theta_2 = 2\delta / H$ and $\varphi = \delta / L_x$; and for the wall with large opening $\theta_1 = \delta / H_y$; $\theta_2 = \delta / (H - H_0)$ and $\varphi = \delta / L_x$.

Equating the internal and external work done gives the following expressions for the uniform in-plane compressive force per unit length:

- For the solid wall

$$n_{uy} = \frac{3m_c H\left(\frac{2L}{H} + \frac{H}{L_x}\right)}{2tL} \tag{29}$$

- For the wall with small opening

$$n_{uy} = \frac{3m_c H\left[\frac{2\left(L - L_0\right)}{H} + \frac{H}{L_x}\right]}{2t\left(L - L_0\right)} \tag{30}$$

- For the wall with large opening

$$n_{uy} = \frac{m_c\left(\frac{H_y + H - H_0}{L_x} + \frac{L_x}{H_y} + \frac{L_x}{H - H_0}\right)}{\frac{t}{3}L_x\left[\frac{H_y + H - H_0}{H_y\left(H - H_0\right)}\right]} \tag{31}$$

The predicted ultimate axial load is calculated according to Eq. (32):

$$N_u = n_{uy}\left(L - L_0\right) \tag{32}$$

The test results are summarized in Table 4, together with the failure loads predicted by the yield-line method. Although the average ratio of predicted to experimental loads was conservative in most cases, the ratios for the CFRP-strengthened walls were somewhat un-conservative. It should be noted that the predicted values were evaluated using a safety factor of 1; in practical applications, the safety factor should be optimized carefully.

4. Concluding Remarks

Design codes treat walls reinforced with minimal amounts of reinforcing material as being unreinforced and predict their ultimate capacity using empirical expressions that assume uniaxial behaviour. As demonstrated by a literature review conducted by the authors of this work, this approach yields very conservative results. Studies on the failure mechanisms of such elements have shown that their lateral restraints transform the failure problem from a one-dimensional problem into a bi-dimensional problem (plate mechanism). Additionally, existing design codes offer limited guidance in situations where new openings must be cut into an existing wall, or where there is a need to apply strengthening using externally bonded reinforcement (i.e. FRP). There is a need for more rigorous treatment of these cases because their inadequate description in current design codes often leads to uncertainties in the design/assessment process.

The paper uses the limit analysis approach to evaluate the failure loads of in- and out-of-plane loaded RC walls with and without openings. The predictions obtained using this approach agree well with experimental data for walls subject to dominant out-of-plane bending. Reasonably good agreement was also achieved for walls under gravitational loads, although some of the predictions in these cases were on the un-safe side because the compressive struts are the main strength component in walls under axial loads (a more complex phenomenon). To account for the effects of transverse strains and material brittleness, the calculated strength must be modified using an appropriate effectiveness factor.

The problem of estimating the elements' strength becomes more complicated if they are strengthened with FRP because the reinforcing fibres exhibit linear-elastic behaviour with no plasticity. As such, their behaviour cannot be described using the plasticity theory. The authors therefore propose an alternative approach whereby the yield criteria for the concrete are updated based on the confined compressive strength due to CFRP-confinement. However, because slender elements and load imperfections are usually encountered in practice, the confinement is generally non-uniform, which limits the effectiveness of the CFRP. An effectiveness factor intended to account for these additional effects was computed based on the experimental observations. However, because this factor was determined using experimental data for only six strengthened walls, further work will be required to validate it. Further work will also be required to validate the model, including tests on walls with different slenderness values, aspect ratios, opening sizes, and opening locations, all of which may affect the yield-line patterns that emerge. In addition, studies could be conducted on walls strengthened with bi- or multi-axial fibres to increase the reliability of the proposed procedure and make it practically useful in assessments.

Notation

A_c	cross-sectional area of concrete
A_e	effective confinement area
A_g	gross area of the cross-section with rounded corners
A_{sx}, A_{sy}	areas of the reinforcement per unit width in the x- and y-directions, respectively
E_c	elastic modulus of concrete
E_{frp}	elastic modulus of CFRP
E_s	elastic modulus of reinforcement
H	height of the wall
H_{eff}	effective height
H_0	height of the cut-out opening
L	length of the wall
L_0	length of the cut-out opening
L_x, L_y	projection of the yield lines onto its axis of rotation in both orthogonal directions
N_{exp}, N_u	experimental/predicted ultimate load for walls under axial loading
R	corner radius
S_{exp}, S_u	experimental/predicted ultimate load for walls under transverse loading
W_E	external work
W_I	internal work
b	width of the virtual cross-section
d	effective depth
f_c	compressive strength of unconfined concrete

f_{cc}	compressive strength of confined concrete
f_{c0}	default value of compressive strength
f_{ct}	tensile strength of concrete
f_{frp}	tensile strength of CFRP
f_l	confining pressure
f_y	yield strength of reinforcement
f_u	tensile strength of reinforcement
h	height of the virtual cross-section
k_1	confinement effectiveness coefficient
k_{s1}	shape factor for strength enhancement
l	length of the yield line
m_b	moment resistance per unit length of the yield line
m_c	membrane moment
m_x, m_y	moment capacities per unit width in the x- and y-directions, respectively
n_{plies}	number of CFRP plies
n_{ux}, n_{uy}	uniform in-plane compressive force per unit length applied in the x- and y-direction, respectively
s	reinforcement spacing
t	thickness of the wall
t_{frp}	single-ply CFRP thickness
w, w_0	experimental/theoretical displacement at the formation of yield-line pattern
x	uncracked depth of the cross-section
α	yield line's inclination relative to the reinforcement
β	effective height factor
δ	virtual displacement
δ_{peak}	out-of-plane displacement at peak load for specimens under eccentric axial loading
ε_{avg}	average strain on CFRP between measurements on the tension and compression side
ε_{cu}	ultimate compressive strain in concrete
ε_{frp}	elongation at break of CFRP
$\varepsilon_{u,frp-max}$, $\varepsilon_{u,frp-min}$	maximum/minimum strain registered on CFRP on a specific location
ϕ_m	curvature
η_{fc}	factor accounting for brittleness of concrete

η_{ε}	factor accounting for influence of transverse cracking
$\eta_{\varepsilon,frp}$	factor accounting for non-uniform confinement
ν	effectiveness factor
θ, φ	angle of disk rotation
ρ_h / ρ_v	horizontal/vertical reinforcement ratio
ρ_{sc}	cross-sectional area ratio of longitudinal steel
σ_c / ε_c	stress/strain in concrete
σ_s / ε_s	stress/strain in steel reinforcement
σ_f / ε_f	stress/strain in FRP
Δ	theoretical out-of-plane displacement under eccentric axial loading

Acknowledgements

The authors would like to acknowledge the Research Council of Norway (RFF), Development Fund of the Swedish Construction Industry (SBUF) and Skanska for financing the work in this project. The authors wish to thank Tech. Lic. Niklas Bagge from Luleå University of Technology for helpful discussions and suggestions. The authors would also like to thank the Swedish branch of Nordea bank for financial support of Cosmin Popescu during an external stay at the Technical University of Denmark.

References

[1] Ali A, Wight J. RC Structural Walls with Staggered Door Openings. J Struct Eng. 1991;117:1514-31.

[2] Taylor CP. Design of slender reinforced concrete walls with openings. ACI Struct J. 1998;95:420-33.

[3] Wang J, Sakashita M, Kono S, Tanaka H. Shear behaviour of reinforced concrete structural walls with eccentric openings under cyclic loading: experimental study. Struct Des Tall Spec. 2012;21:669-81.

[4] Todut C, Dan D, Stoian V. Theoretical and experimental study on precast reinforced concrete wall panels subjected to shear force. Eng Struct. 2014;80:323-38.

[5] Mosoarca M. Failure analysis of RC shear walls with staggered openings under seismic loads. Eng Fail Anal. 2014;41:48-64.

[6] Mosallam AS, Nasr A. Structural performance of RC shear walls with post-construction openings strengthened with FRP composite laminates. Compos Part B-Eng. 2017;115:488-504.
[7] Popescu C, Sas G, Blanksvärd T, Täljsten B. Concrete walls weakened by openings as compression members: A review. Eng Struct. 2015;89:172-90.
[8] Pillai SU, Parthasarathy CV. Ultimate strength and design of concrete walls. Build Environ. 1977;12:25-9.
[9] Saheb M, Desayi P. Ultimate strength of RC wall panels in one-way in-plane action. J Struct Eng. 1989;115:2617-30.
[10] Fragomeni S. Design of Normal and High Strength Reinforced Concrete Walls [PhD Thesis]. Melbourne, Australia: Univ. of Melbourne; 1995.
[11] Doh JH. Experimental and Theoretical Studies of Normal and High Strength Concrete Wall Panels [PhD Thesis]. Gold Coast, Australia: Griffith Univ.; 2002.
[12] Ganesan N, Indira PV, Santhakumar A. Prediction of ultimate strength of reinforced geopolymer concrete wall panels in one-way action. Constr Build Mater. 2013;48:91-7.
[13] Robinson G, Palmeri A, Austin S. Design methodologies for one way spanning eccentrically loaded minimally or centrally reinforced pre-cast RC panels. Eng Struct. 2013;56:1945-56.
[14] Swartz SE, Rosebraugh VH, Rogacki SA. A method for determining the buckling strength of concrete panels. Exp Mech. 1974;14:138-44.
[15] Sanjayan JG. Load capacity of slender high-strength concrete walls with side supports. ACI Struct J. 1999;96:571-6.
[16] Saheb M, Desayi P. Ultimate Strength of R.C. Wall Panels in Two- Way In- Plane Action. J Struct Eng. 1990;116:1384-402.
[17] Saheb M, Desayi P. Ultimate strength of RC wall panels with openings. J Struct Eng. 1990;116:1565-78.
[18] Doh JH, Fragomeni S. Ultimate load formula for reinforced concrete wall panels with openings. Adv Struct Eng. 2006;9:103-15.
[19] Lee D-J. Experimental and theoretical study of normal and high strength concrete wall panels with openings [PhD Thesis]. Gold Coast, Australia: Griffith Univ.; 2008.
[20] Mohammed B, Ean LW, Malek MA. One way RC wall panels with openings strengthened with CFRP. Constr Build Mater. 2013;40:575-83.
[21] Doh J, Fragomeni S. Evaluation of experimental work on concrete walls in one-way and two-way action. Austr J Struct Eng. 2005;6:37–52.
[22] Aghayere AO, MacGregor JG. Analysis of concrete plates under combined in-plane and transverse loads. ACI Struct J. 1990;87:539-47.
[23] Hegger J, Dressen T, Will N. Load-bearing capacity of plain concrete walls. Mag Concrete Res. 2009;61:173-82.
[24] Guan H, Cooper C, Lee D-J. Ultimate strength analysis of normal and high strength concrete wall panels with varying opening configurations. Eng Struct. 2010;32:1341-55.
[25] Lima MM, Doh J-H, Hadi MNS, Miller D. The effects of CFRP orientation on the strengthening of reinforced concrete structures. Struct Des Tall Spec. 2016;25:759-84.
[26] Ho N-M, Doh J-H, Fragomeni S. Instability analysis of reinforced concrete walls with various support conditions. Struct Des Tall Spec. 2017;26:e1353-n/a.

[27] EN1992-1-1. Design of concrete structures – Part 1–1: General rules and rules for buildings. Brussels, Belgium: CEN (European Committee for Standardization); 2004.
[28] ACI 318. Building code requirements for structural concrete and commentary Farmington Hills, MI: American Concrete Institute (ACI); 2011.
[29] AS3600. Concrete structures. Sydney, Australia: Standards Australia; 2009.
[30] DIN 1045. Reinforced concrete structures: Design and construction. Berlin: DIN (Deutsches Institut für Normung); 1988.
[31] Ganesan N, Indira PV, Rajendra Prasad S. Strength and Behavior of SFRSCC and SFRC Wall Panels under One-Way In-Plane Action. In: Parra-Montesinos G, Reinhardt H, Naaman AE, editors. High Performance Fiber Reinforced Cement Composites 6: Springer Netherlands; 2012. p. 279-86.
[32] Sadiki M, Reenberg AM. Tværbelastede vægelementer [Master thesis]. Lyngby, Denmark: Technical Univ. of Denmark; 2013.
[33] Popescu C, Sas G, Sabău C, Blanksvärd T. Effect of cut-out openings on the axial strength of concrete walls. J Struct Eng. 2016;*142*:04016100.
[34] Popescu C, Sas G, Blanksvärd T, Täljsten B. Concrete walls with cutout openings strengthened by FRP-confinement. Journal of Composites for Construction. 2017;*21*:04016106.
[35] ACI 224R-01. Control of Cracking in Concrete Structures. American Concrete Institute (ACI). ACI Committee 224.; 2001.
[36] SS-EN ISO 898-1. Mechanical properties of fasteners made of carbon steel and alloy steel - Part 1: Bolts, screws and studs with specified property classes - Coarse thread and fine pitch thread (ISO 898-1:2013). Stockholm, Sweden: Swedish Standards Institute (SIS); 2013.
[37] Lam L, Teng JG. Design-Oriented Stress-Strain Model for FRP-Confined Concrete in Rectangular Columns. J Reinf Plast Comp. 2003;22:1149-86.
[38] Bailey CG, Toh WS. Small-scale concrete slab tests at ambient and elevated temperatures. Eng Struct. 2007;29:2775-91.
[39] fib Model Code 2010. fib Model Code 2010 for Concrete Structures. Lausanne, Switzerland: Fédération Internationale du Béton; 2013.
[40] Floruţ S-C, Sas G, Popescu C, Stoian V. Tests on reinforced concrete slabs with cut-out openings strengthened with fibre-reinforced polymers. Compos Part B-Eng. 2014;66C:484–93.
[41] Ingerslev A. The strength of rectangular slabs. J Inst Struct Eng. 1923;1:3–14.
[42] Johansen KW. Yield line theory. London: Cement and Concrete Association; 1962.
[43] Hansen LZ. Unreinforced Masonry Walls Transversely and Axially Loaded [PhD Thesis]. Lyngby, Denmark: Technical Univ. of Denmark; 2004.
[44] Nielsen MP. Limit analysis and concrete plasticity, Second Edition. Boca Raton, FL: CRC Press; 1999.
[45] Wang Y, Dong Y-L, Yuan G-L, Zou C-Y. New failure criterion to determine the load carrying capacity of two-way reinforced concrete slabs. Adv Struct Eng. 2015;18:221-36.
[46] Bailey CG, Toh WS, Chan BM. Simplified and Advanced Analysis of Membrane Action of Concrete Slabs. ACI Struct J. 2008;105:30-40.

[47] Gere JM, Timoshenko SP. Mechanics of materials, 3rd ed. Massachusetts, USA: PWS-KENT; 1990.
[48] Popescu C, Sas G. The development of an experimental program through design of experiments and FEM analysis: A preliminary study. Nord Concrete Res. 2014;51:29-42.
[49] Cervenka Consulting Ltd. ATENA - Advanced Tool for Engineering Nonlinear Analysis. Prague, Czech Republic 2015.

List of figures

List of tables

Table 1

Click here to download Table: Table 1.docx

Table 1. Summary of tested specimens

<table>
<tr><th>Wall</th><th>L (m)</th><th>H (m)</th><th>t (m)</th><th>L_0 (m)</th><th>H_0 [a] (m)</th><th>f_c [b] (MPa)</th><th>ρ_h (%)</th><th>ρ_v (%)</th><th>f_y (MPa)</th><th>f_u (MPa)</th><th>δ_{peak} [c] (mm)</th><th>S_{exp} (kN/m^2)</th><th>N_{exp} (kN)</th></tr>
<tr><td colspan="14">Walls under transversal load</td></tr>
<tr><td>A</td><td rowspan="6">4.0</td><td rowspan="6">2.6</td><td rowspan="6">0.1</td><td>-</td><td>-</td><td>49.7</td><td>0.196</td><td>0.190</td><td>600</td><td>662</td><td>81.81</td><td>21.2</td><td rowspan="6">-</td></tr>
<tr><td>B</td><td>-</td><td>-</td><td>49.7</td><td>0.196</td><td>0.190</td><td>600</td><td>662</td><td>73.08</td><td>21.8</td></tr>
<tr><td>C</td><td>1.3</td><td>1.0</td><td>49.7</td><td>0.196</td><td>0.190</td><td>600</td><td>662</td><td>125.19</td><td>15.3</td></tr>
<tr><td>D</td><td>1.3</td><td>1.0</td><td>49.7</td><td>0.196</td><td>0.190</td><td>600</td><td>662</td><td>109.51</td><td>17.0</td></tr>
<tr><td>E</td><td>1.3</td><td>1.0</td><td>49.7</td><td>0.136</td><td>0.133</td><td>651</td><td>701</td><td>115.85</td><td>11.0</td></tr>
<tr><td>F</td><td>1.3</td><td>1.0</td><td>49.7</td><td>0.136</td><td>0.133</td><td>651</td><td>701</td><td>108.74</td><td>12.3</td></tr>
<tr><td colspan="14">Loads under eccentric axial load</td></tr>
<tr><td>I-C</td><td rowspan="9">1.8</td><td rowspan="9">1.35</td><td rowspan="9">0.06</td><td>-</td><td>-</td><td>62.8</td><td>0.339</td><td>0.327</td><td>632</td><td>693</td><td>18.96</td><td rowspan="9">-</td><td>2363</td></tr>
<tr><td>I-S</td><td>0.45</td><td>1.05</td><td>62.8</td><td>0.339</td><td>0.327</td><td>632</td><td>693</td><td>26.67</td><td>1500</td></tr>
<tr><td>I-L</td><td>0.90</td><td>1.05</td><td>62.8</td><td>0.339</td><td>0.327</td><td>632</td><td>693</td><td>11.18</td><td>1180</td></tr>
<tr><td>II-S</td><td>0.45</td><td>1.05</td><td>62.8</td><td>0.339</td><td>0.327</td><td>632</td><td>693</td><td>22.35</td><td>2241</td></tr>
<tr><td>II-L</td><td>0.90</td><td>1.05</td><td>62.8</td><td>0.339</td><td>0.327</td><td>632</td><td>693</td><td>5.84</td><td>1497</td></tr>
<tr><td>III-S1</td><td>0.45</td><td>1.05</td><td>64.4</td><td>0.339</td><td>0.327</td><td>632</td><td>693</td><td>21.73</td><td>2178</td></tr>
<tr><td>III-S2</td><td>0.45</td><td>1.05</td><td>64.4</td><td>0.339</td><td>0.327</td><td>632</td><td>693</td><td>17.41</td><td>2009</td></tr>
<tr><td>III-L1</td><td>0.90</td><td>1.05</td><td>64.4</td><td>0.339</td><td>0.327</td><td>632</td><td>693</td><td>12.34</td><td>1334</td></tr>
<tr><td>III-L2</td><td>0.90</td><td>1.05</td><td>64.4</td><td>0.339</td><td>0.327</td><td>632</td><td>693</td><td>7.31</td><td>1482</td></tr>
</table>

[a] Heights of window- and door-type openings in walls under transverse and axial loading, respectively

[b] Mean compressive strength determined based on cylinder and cube tests for walls under transverse and axial loading, respectively. A conversion factor of 0.83 is used in later calculations to convert the cube compressive strength into cylinder compressive strength.

[c] Maximum out-of-plane displacements at peak load: measurements in the mid-point location for solid walls and at the opening edge for specimens with openings

Table 2

Click here to download Table: Table 2.docx

Table 2. Characteristics of the CFRP and its adhesive

Property	Epoxy adhesive (StoPox LH)	CFRP ply (StoFRP IMS300 C300)
Single-ply thickness, t_{frp} (mm)	-	0.17
Tensile strength, f_{frp} (MPa)	>60	>5500
Elastic modulus, E_{frp} (GPa)	2	290
Elongation at break, ε_{frp} (%)	3	1.9

Table 3
Click here to download Table: Table 3.docx

Table 3. Experimental ultimate transverse loads and yield line predictions obtained with and without consideration of the effects of strain hardening

Wall	Ultimate transverse load (kN/m^2)				
	Experimental (S_{exp})	Predicted (S_u)			
		No strain hardening	Accuracy S_u/S_{exp}	Strain hardening	Accuracy S_u/S_{exp}
A	21.2	18.37	0.87	20.23	0.95
B	21.8	18.37	0.84	20.23	0.93
C	15.3	13.24	0.87	14.59	0.95
D	17.0	13.24	0.78	14.59	0.86
E	11.0	10.10	0.92	10.86	0.99
F	12.3	10.10	0.82	10.86	0.88
Average			0.85		0.93
CoV (%)			5.5		5.2

Table 4. Comparison of measured ultimate axial loads and yield line predictions

Wall	Ultimate axial load (kN)		Accuracy
	Experimental (N_{exp})	Predicted (N_u)	N_u/N_{exp}
I-C	2363	1872	0.79
I-S	1500	1325	0.88
I-L	1180	1046	0.89
II-S	2241	1979	0.88
II-L	1497	1527	1.02
III-S1	2178	2072	0.95
III-S2	2009	2567	1.28
III-L1	1334	1198	0.90
III-L2	1482	1464	0.99
Average			0.95
CoV (%)			14.6

Figure 1

Click here to download Figure: Figure 1.pdf

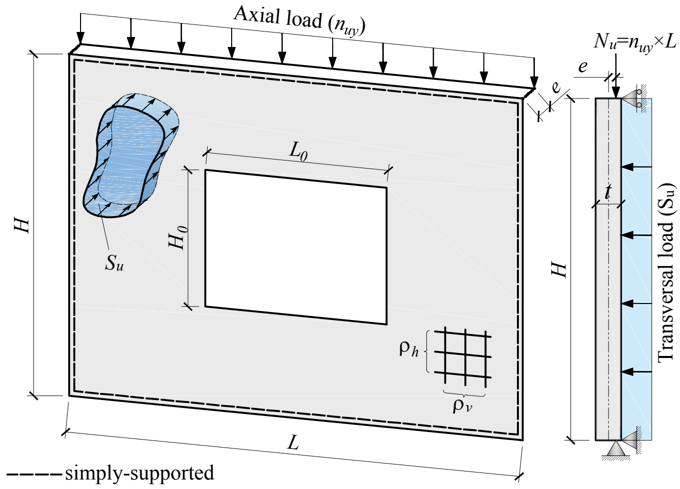

Figure 2

Click here to download Figure: Figure 2.pdf

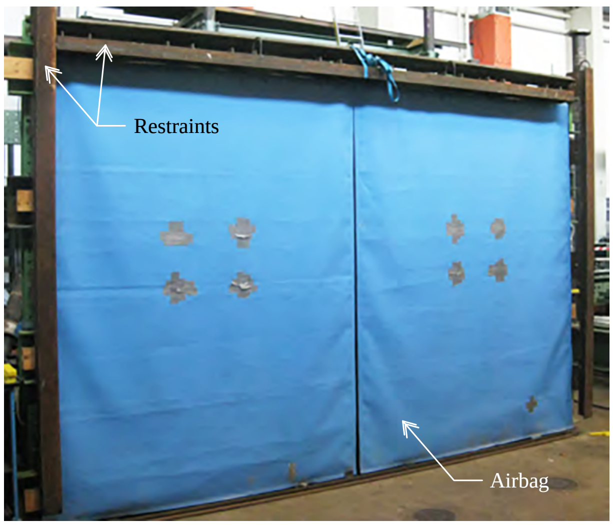

Figure 3
Click here to download Figure: Figure 3.pdf

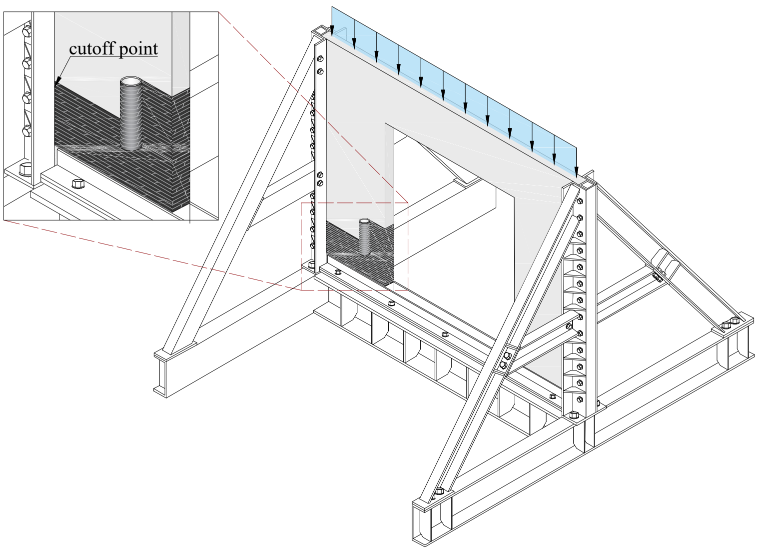

Figure 4

Click here to download Figure: Figure 4.pdf

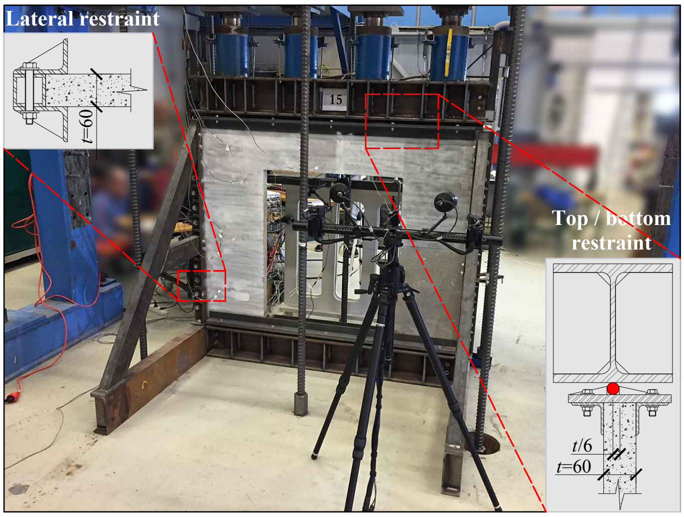

Figure 5

Click here to download Figure: Figure 5.pdf

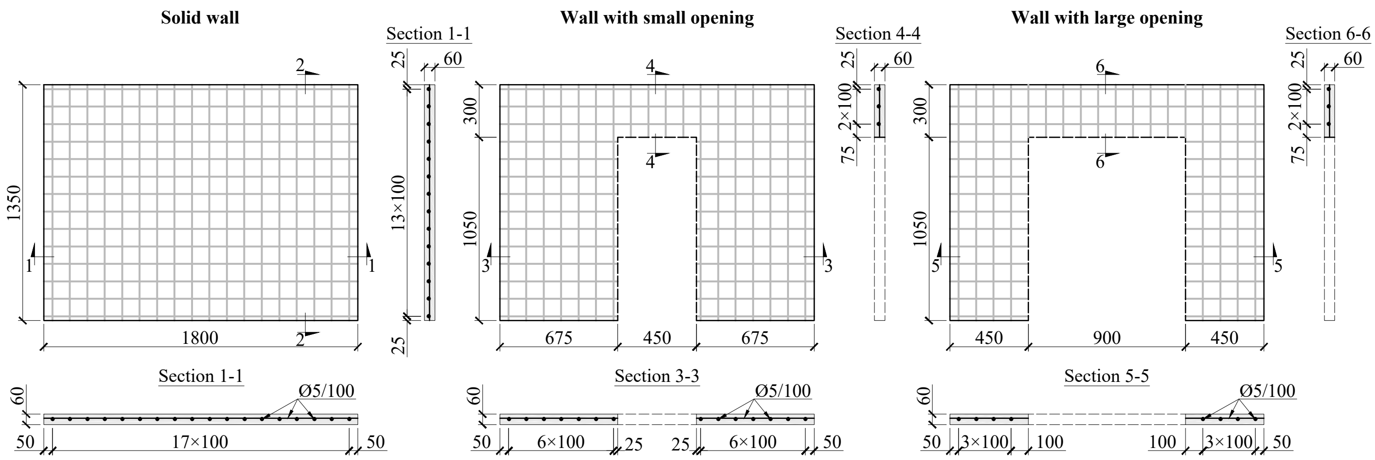

Figure 6

Click here to download Figure: Figure 6.pdf

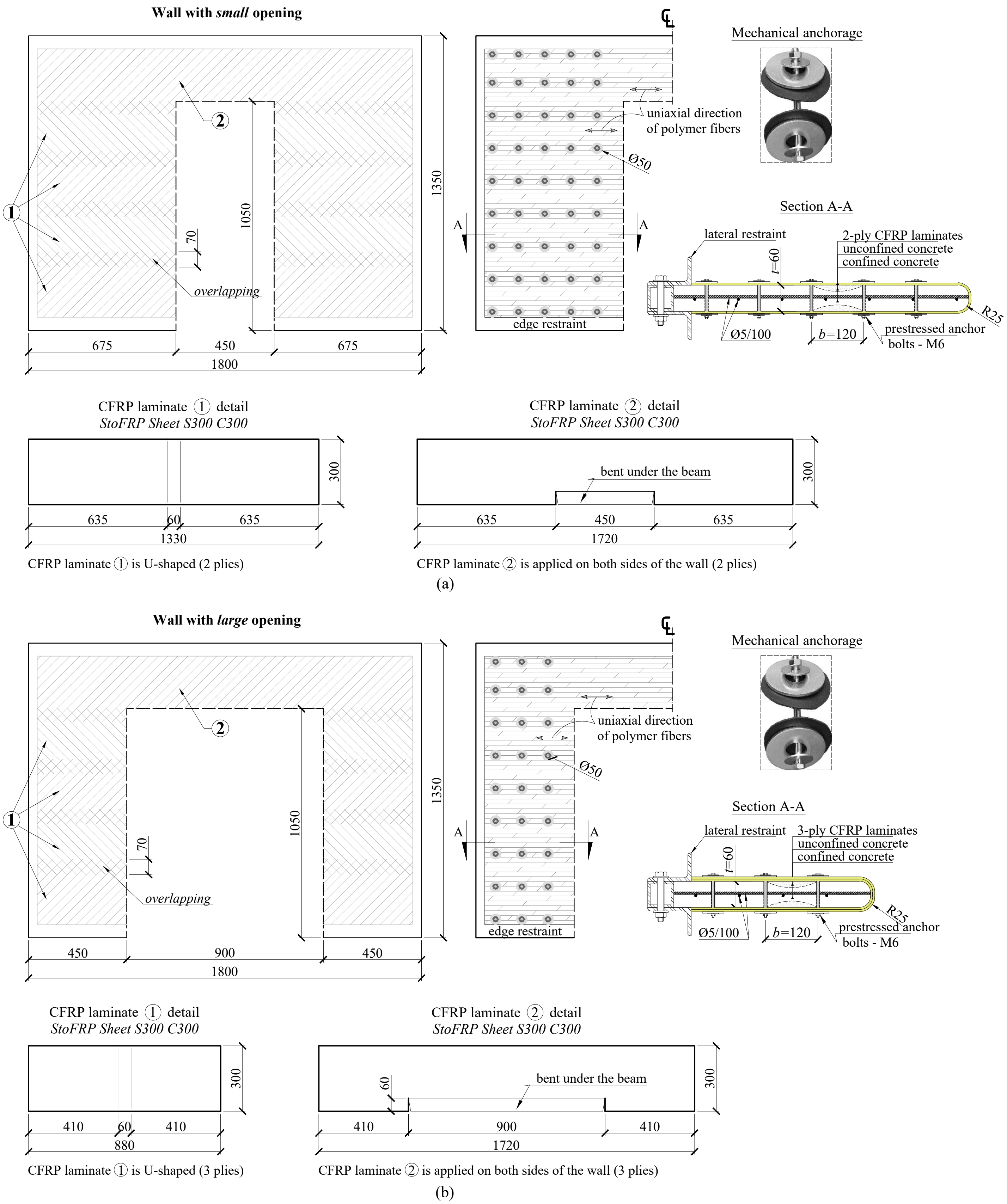

Figure 7
Click here to download Figure: Figure 7.pdf

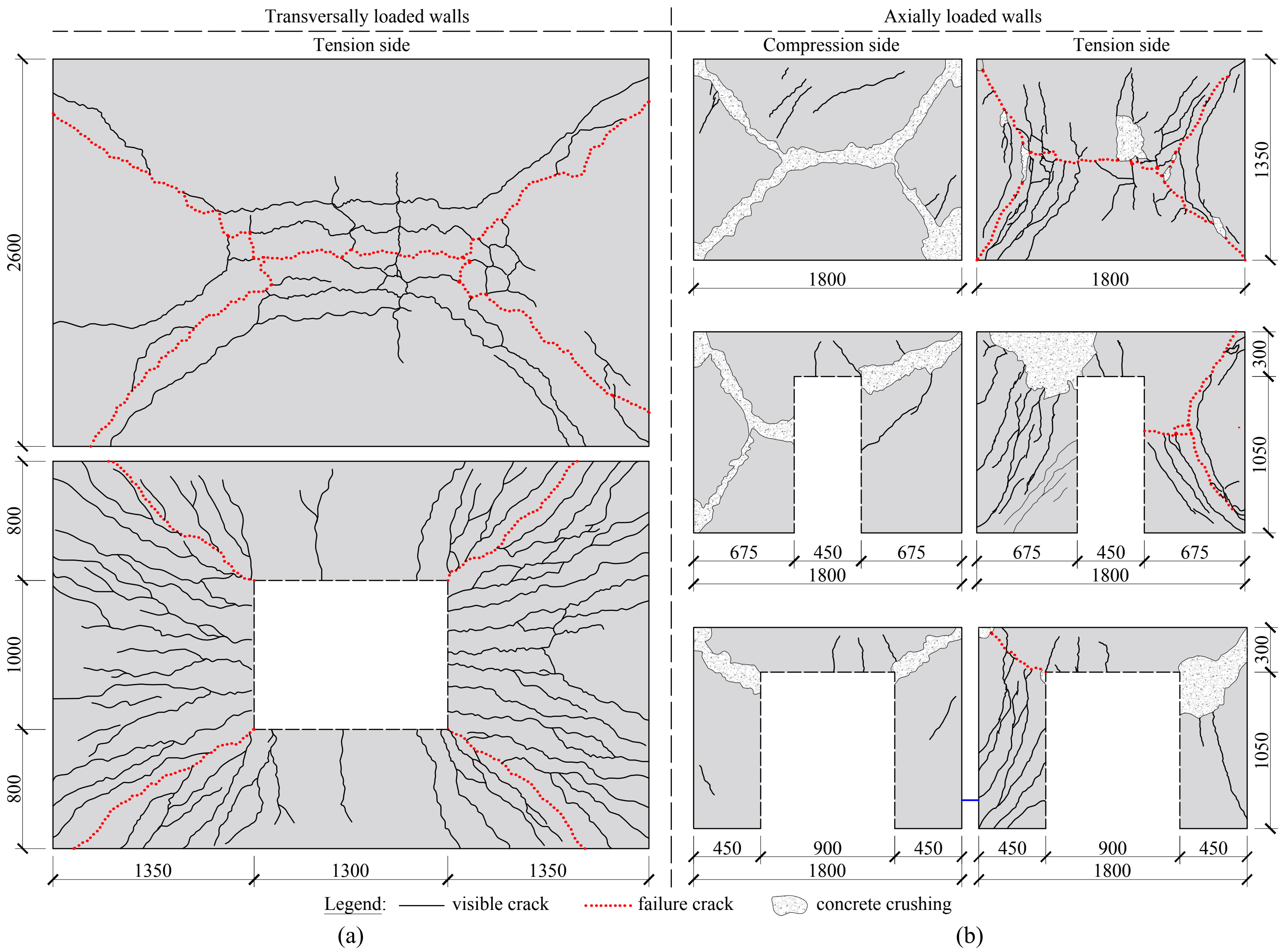

Figure 8
Click here to download Figure: Figure 8.pdf

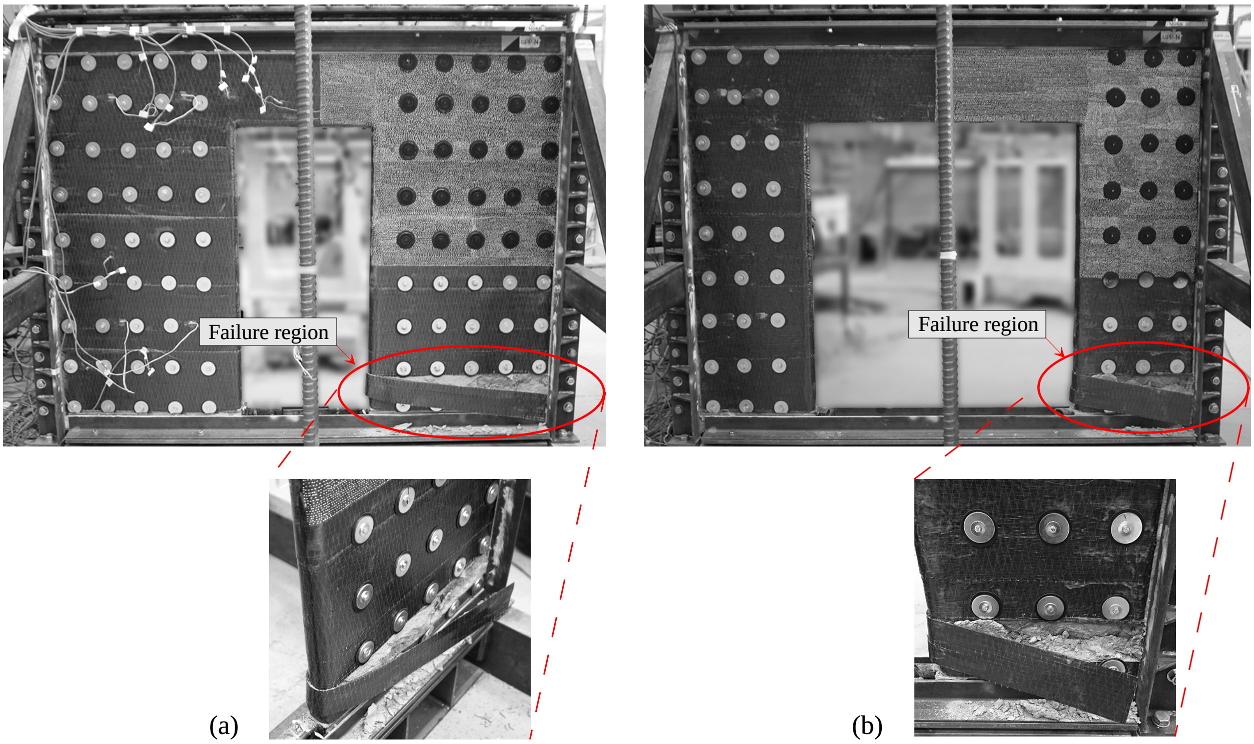

Figure 9
Click here to download Figure: Figure 9.pdf

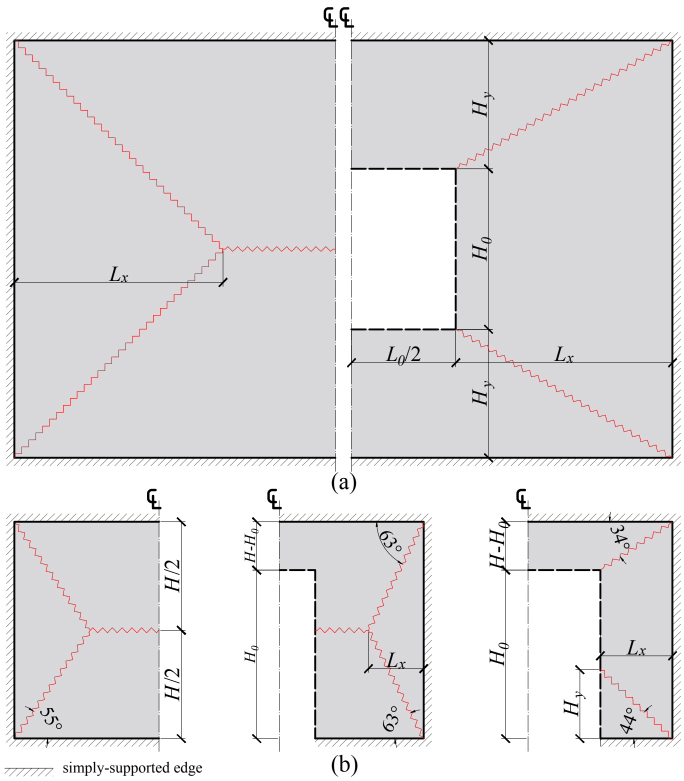

Figure 10

Click here to download Figure: Figure 10.pdf

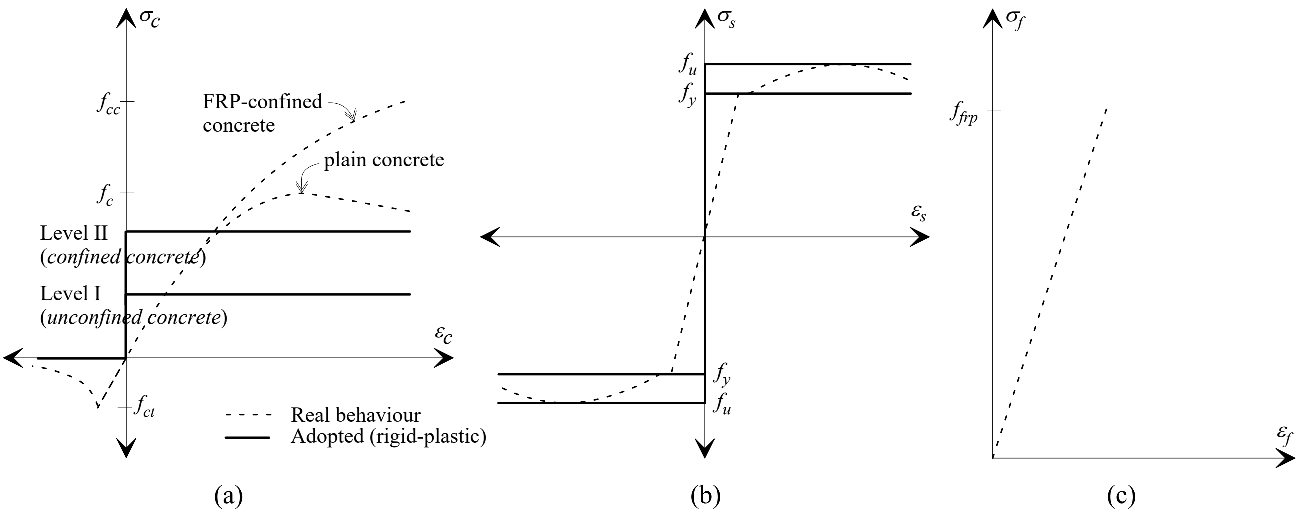

Figure 11

Click here to download Figure: Figure 11.pdf

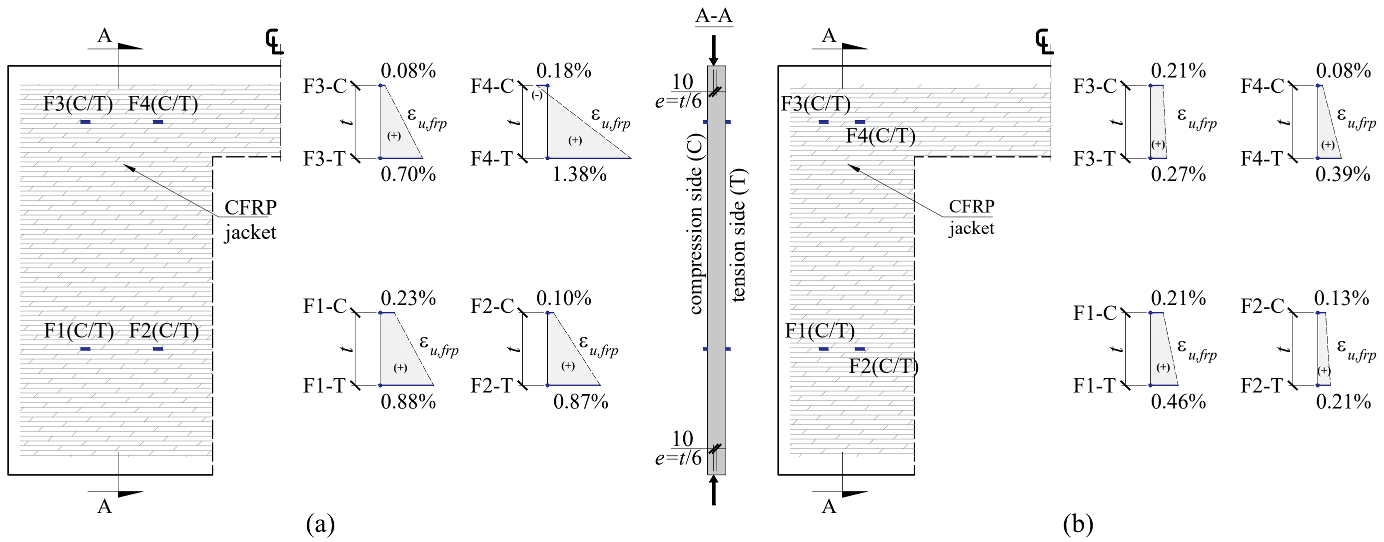

Figure 12
Click here to download Figure: Figure 12.pdf

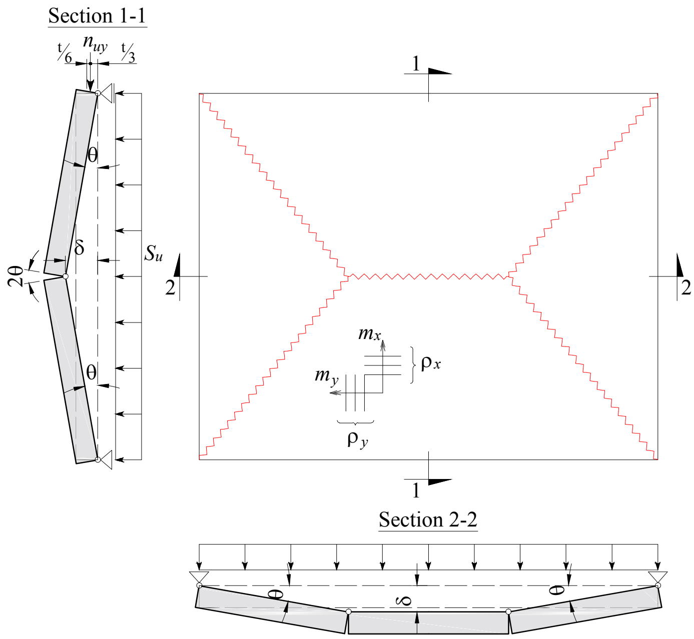

Figure 13

Click here to download Figure: Figure 13.pdf

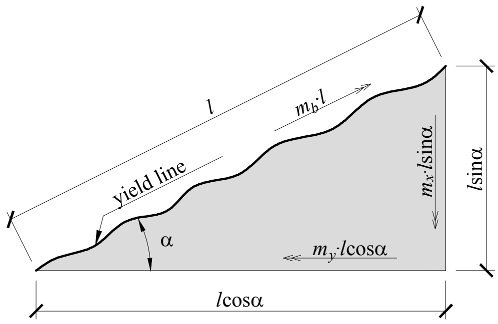

Figure 14

Click here to download Figure: Figure 14.pdf